Journal of Thermal Analysis and Calorimetry (2018) 134:51–57
https://doi.org/10.1007/s10973-018-7417-2

The study of thermal, microstructural and magnetic properties of manganese–zinc ferrite prepared by co-precipitation method using different precipitants

Irena Szczygieł[1] · Katarzyna Winiarska[1] · Agnieszka Sobianowska-Turek[2]

Received: 30 October 2017 / Accepted: 25 May 2018 / Published online: 4 June 2018

Abstract
Mn–Zn ferrite was prepared from the solution after acid leaching of spent batteries by co-precipitation method using ammonia oxalate, sodium carbonate and sodium hydroxide as precipitating agents. The co-precipitation process was performed at temperature of over 50 °C by continuous magnetic stirring. The precipitates were pre-sintered at 850 °C in air. Dilatometric study has revealed that lowest shrinkage (only 5.6%) showed a material obtained from an oxalate precipitant. After pressing and high-temperature sintering at 1325 °C, it showed both insufficient density and the presence of pores, which contribute to the deterioration in the magnetic properties of the ferrites: the low magnetic permeability value and high magnetic losses. Ferrite prepared from hydroxide and carbonate precipitant showed a much higher shrinkage, sintered density and much higher magnetic permeability compared with the ferrite prepared from oxalate precursor.

Keywords Mn–Zn ferrite · Co-precipitation · Battery scrap · Microstructure · Magnetic properties · TGA–DTA/DIL/XRD/SEM

Introduction

Mn–Zn ferrites are important group of soft magnetic materials commonly used in microelectronics, e.g., in transformer cores, choke coils and electromagnetic interference devices (EMI). High initial magnetic permeability, electrical resistivity and low core losses at high frequencies are the most important properties determining the scope of their applicability. The magnetic properties of Mn–Zn ferrites exploited in a particular application depend on their structure (crystal structure and elemental composition) and microstructure (density, porosity, the size and shape of particles and pores) which are determined by the synthesis conditions, such as the sintering time and temperature. On the industrial scale, ferrites are produced by the ceramic method. The bottom-up nanotechnology approach, including soft chemical method, allows to synthesize homogeneous materials with defined morphology. Among these methods, especially sol–gel autocombustion [1–6], co-precipitation [7, 8], the hydrothermal and solvothermal [9–11], the reverse micelles [12] and the mechanochemical [13] methods have been extensively studied in the last years. Ferrite produced by chemical methods is often characterized by unique properties suitable for new advanced application, i.e., magnetic high-density information storage or drug delivery or contrast agent in biomedicine [14–18]. Ferrite powders obtained by low-temperature synthesis due to their metastable character and high activity can be used in catalysis [3, 19, 20]. Besides the research on ferrite preparation by chemical methods, there are reports of the possibility of Mn–Zn ferrites synthesis from battery waste [21–29]. Battery scrap, especially

Electronic supplementary material The online version of this article (https://doi.org/10.1007/s10973-018-7417-2) contains supplementary material, which is available to authorized users.

✉ Katarzyna Winiarska
katarzyna.winiarska@ue.wroc.pl

[1] Department of Inorganic Chemistry, Faculty of Engineering and Economics, Wrocław University of Economics, Komandorska 118/120, 53-345 Wrocław, Poland

[2] Division on Waste Technology and Land Remediation, Faculty of Environmental Engineering, Wrocław University of Science and Technology, Wybrzeże Wyspiańskiego 27, Wrocław, Poland

Zn–C and Zn–Mn battery, due to its qualitative and quantitative composition is the ideal by-product for receiving Mn–Zn ferrite. Both in Poland and in Europe, processing of waste batteries and accumulators is still an important aspect of waste management. The Directive of the European Parliament and of the Council of 26 September 2006 [30] defines the minimum levels of collection and recycling of waste batteries and accumulators and encourages to create new technologies of their processing. Proposed in the literature methods of treating used batteries rely on mechanical crushing and then leaching with sulfuric [21, 22], hydrochloric [23] or nitric acid [24, 25]. Ferrite can be prepared from such solutions by co-precipitation [26–28] or by combustion methods in the presence of citric acid (as a fuel) and nitrate ions, usually derived from nitric acid leaching of crushed battery waste (as an oxidant) [24, 25, 29]. The degree of leaching Mn, Zn and Fe—main components of ferrite, and the microstructure and phase composition of the obtained product were studied, but only Nan et al. [21] and Kim et al. [27] characterized the magnetic properties of ferrites prepared from waste battery. They found that saturation magnetization of the powders obtained by co-precipitation is similar to that of Mn–Zn ferrites synthesized by other chemical methods.

The aim of this study is synthesis of Mn–Zn ferrites by co-precipitation from the solution after acid leaching of battery waste and determination of the effect of the applied precipitating agents on the thermal, microstructural and magnetic properties of the obtained powders. The solution after leaching of battery mass by sulfuric acid is rich in Zn and Mn ions and enriched in a stoichiometric amount of $FeSO_4$, a good source to prepare microcrystalline Mn–Zn ferrites. The effect of the grain size of the ferrite powders on shrinkage during sintering of compressed samples and magnetic properties is discussed in the paper.

Experimental

Mn–Zn ferrite preparation

Mn–Zn ferrites were obtained from solution after battery scrap leaching with the sulfuric acid (VI). A detailed description of the leaching process containing the selection of leaching parameters is given in [31, 32]. The degree of leaching was ~ 85–95% for zinc and 25–30% for manganese. Therefore, the solution was enriched with appropriate amount of manganese(II) and iron(II) sulfates in order to get the $Mn_{0.6}Zn_{0.4}Fe_2O_4$ stoichiometry. Co-precipitation was performed under previously predetermined conditions for three precipitants: ammonium oxalate (T = 60 °C, t = 1.5 h, pH = 4, sample denoted as "*S*1"), sodium carbonate (T = 50 °C, t = 3 h, pH = 8.5, sample denoted as "*S*2") and sodium hydroxide (T = 60 °C, t = 3 h, pH = 10, sample denoted as "*S*3"). A precipitating agent was added sequentially to the solution and, if required, the pH of the mixture was adjusted with the use of ammonia 25 vol%. The obtained suspension was heated under continuous magnetic stirring. The precipitates were then filtered under reduced pressure and thoroughly washed with distilled water to remove the remaining sulfates. The received sludge was dried in a drying chamber at 105 °C for 24 h, and then, it was subjected to a typical procedure like ceramic ferrites: pre-sintering at 850 °C, grinding, pressing and at last sintering during the final microstructural and magnetic properties are achieved. The finishing sintering process was carried out at 1325 °C for 3 h in an oxygen atmosphere. Oxygen partial pressure was controlled according to procedure given by Schaller [33] and Morineau et al. [34].

Mn–Zn ferrite characterization

Identification and phase composition of prepared ferrite powders were determined by X-ray diffraction analysis at room temperature on Siemens D-500 Diffractometer (with radiation CuKα and wavelength 1.54051 Å). The X-ray diffraction data were obtained at the angles 5–80° with a step of 0.04° and time 1 s per step. The phases were identified by utilizing the ICDD PDF-4 database. Scanning electron microscopy (FEI Quanta^{TM}250) allowed to determine a morphology and grains' size. All the samples for scanning electron microscopic observation were previously sputtered with a thin (~ 10 nm) layer of carbon. Thermoanalytical analysis (DTA/DTG/TGA) was carried out with a derivatograph type 3427 (MOM, Hungary), from 20 °C up to 1350 °C under air (heating rate: 7.5 °C min^{-1}, reference material: α-alumina, platinum crucibles, Pt/PtRh10 thermocouple). Dimensional changes of ferrite powders were provided by dilatometry (DIL) on the DIL 402 dilatometer (Netzsch) in the temperature range of 25–1300 °C with a step of 2° min^{-1}. The powders were compressed into pellets (with addition 10 vol% of WAX binder) and heated up to 1300 °C. For magnetic testing, ferrite powders after pre-sintering at 850 °C were pressed into toroidal rings. The density of the finally sintered toroidal specimens was measured by Archimedes water density method. The magnetic properties were performed on an EMMA device. The power losses were measured at 25 kHz under magnetic field of 200 mT. Loss factor was investigated in 25 °C, 0.1 mT and frequency range of 25–1000 Hz. Permeability was tested in a frequency range of 25–1000 Hz and field 0.1 mT in two independent measurements at constant temperature of 25 °C or variable temperature in the 25–85 °C range.

Results

DTA–TGA analysis performed on precipitates obtained from ammonia oxalate, sodium carbonate and sodium hydroxide enabled to determine the conditions of pre-sintering and final sintering of powders. In the DTA–TGA heating curves for the oxalate precipitate, two thermal effects at onset temperatures of ~ 200 °C and maximum at 280 °C appeared (Fig. 1a). The first endothermic effect is associated with the dehydration of the precipitated powder. The next, exothermic effect at 280 °C is associated with the decomposition of precipitate and formation of oxides. The exothermal reaction is accompanied by a significant mass loss of approximately 55%. Above 400 °C, TGA curve did not show any mass change. A slight exothermic effect on the DTA curve at about 1300 °C indicates that the spinel phase is ultimately formed at this temperature. The carbonate deposit (Fig. 1b) undergoes dehydration at about 100 °C and a significant mass loss (about 25%) observed at TGA curve begins and finally ends at 850 °C. At 280 °C, there is a pronounced endothermic effect on the DTA curve associated with the decomposition of carbonates into the oxides. Also, a small exothermic effect was observed for this sample at about 1300 °C. For the hydroxide precipitate (Fig. 1c), small changes are visible on the DTA curve. They are connected with a slight mass loss of approximately 7% in 200–400 °C range (TGA). Dehydration, which was associated with the partial oxidation of Mn, Zn and Fe, occurs in this temperature range. There is no mass change above 400 °C at TGA curve. Similar to the previously described oxalate and carbonate precipitates, a small exothermic effect was observed at ~ 1300 °C. Based on the conducted DTA/TGA research, there was established final sintering temperature of the precipitates as 1325 °C.

The relative contribution of each oxide in Mn–Zn ferrite obtained from solution after battery waste leaching and finally sintered at 1325 °C was investigated by X-ray fluorescence spectroscopy method (XRF). On the basis of analysis data (Table 1), it can be concluded that relative contribution of main ferrite oxides: Fe_2O_3, MnO and ZnO, is close to the expected composition ($Mn_{0.6}Zn_{0.4}Fe_2O_4$). The iron oxide contribution in sample prepared from hydroxide precipitate (*S*3) was slightly lower than in others samples. The Zn–C and Zn–Mn waste battery stream besides Zn, Mn and Fe usually contains other elements [35]. Therefore, the amount of other metal oxides from battery scrap in prepared materials was determined and is listed in Table 1. The MgO content in the *S*1 and *S*3 samples exceeded 3%, whereas in *S*2 sample it amounted to nearly 1%. SiO_2, TiO_2 and CaO amounts were not higher than 0.5%. It should be noted that the contribution of other impurities (Co, Cu, Ni oxides) was small; however, their presence may contribute to deterioration in structural and magnetic properties in Mn–Zn ferrite. Considering the higher than expected magnesia (MgO) content (see Table 1), the composition of the obtained materials can be described as formulas: $Mn_{0.52}Zn_{0.38}Mg_{0.10}Fe_2O_4$ (for samples *S*1 and *S*3) and $Mn_{0.56}Zn_{0.41}Mg_{0.03}Fe_2O_4$ (for *S*2 sample).

The ferrite powders after pre-sintering at 850 °C are almost two phases. The X-ray diffraction analysis (Supplementary material 1) revealed that apart from spinel phase, an α-hematite is crystallized. The relative mass fraction of the non-magnetic phase in the pre-sintered ferrites was determined on the basis of the ratio of the

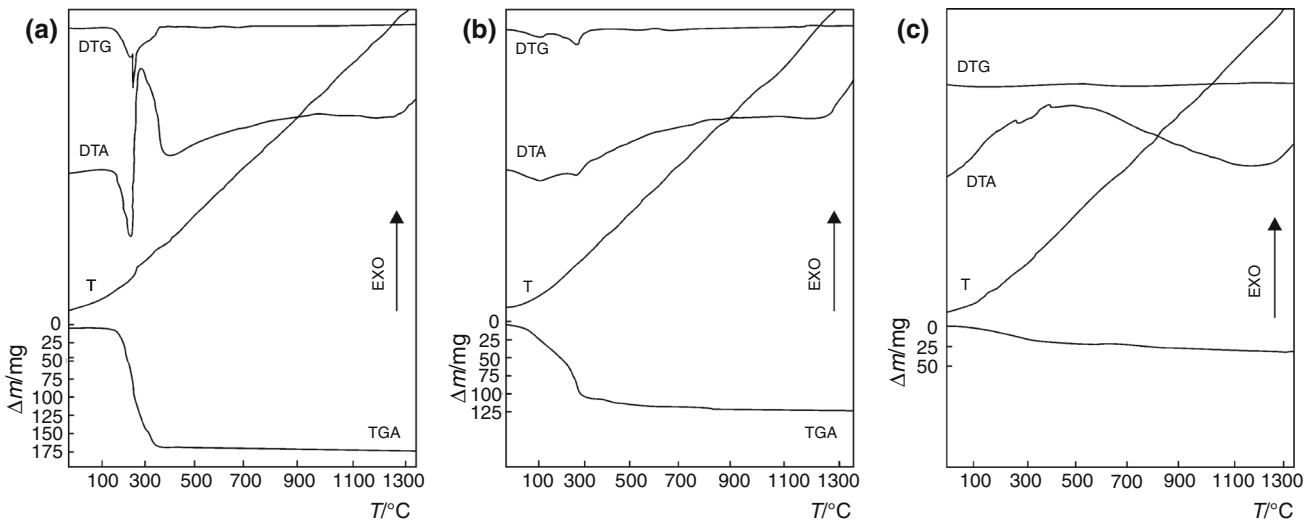

Fig. 1 The DTA/DTG/TGA curves of precipitates prepared using **a** ammonia oxalate, **b** sodium carbonate, **c** sodium hydroxide as precipitating agent

Table 1 Relative contribution of metal oxides in prepared ferrites

Sample	%Fe_2O_3	%MnO	%ZnO	%TiO_2	%CaO	%SiO_2	%CoO	%CuO	%NiO	%MgO	%Al_2O_3
*S*1	67.76	18.76	13.45	0.034	0.177	0.202	0.020	0.020	0.064	3.640	0.017
*S*2	67.11	18.76	13.78	0.325	0.189	0.258	0.017	0.046	0.067	0.970	0.067
*S*3	66.82	18.90	13.95	0.334	0.055	0.274	0.018	0.044	0.067	3.520	0.069

major hematite-derived peaks intensity to the intensity of peak characteristic for the spinel phase. Ferrite powder prepared from oxalate precipitate (*S*1) was characterized by the smallest part of hematite amounted at about 10%, whereas the ferrite prepared from carbonate precursor (*S*2) included 25% of hematite. Slightly lower (20%) hematite part was in *S*3 sample, which was synthesized by the use of sodium hydroxide as precipitating agent. The XRD patterns of ferrite samples sintered at 1325 °C in controlled oxygen atmosphere are shown in Fig. 2. The diffraction peaks are slightly shifted toward lower 2Θ angles compared with diffraction peaks' position for spinel cubic structure of Mn–Zn ferrite (JCPDS-ICDD Card No. 01-074-2401). In addition, the peaks at higher angles have greater shift (but not the same 2Θ value) compared with those at smaller 2Θ values. According to the Bragg's law, it suggests an expansion of the spinel unit cell. An increase in cubic spinel lattice can be caused by the incorporation of other cations (as impurities) from the solution after leaching into the spinel lattice. The XRD reflections originating in these secondary phases are not visible in the XRD patterns, because their content is beyond the detection level for the powder XRD method, despite the fact that the XRF shows a presence of other metal oxides.

A linear shrinkage for initially sintered at 850 °C and then pressed ferrite powders prepared by co-precipitation was investigated by dilatometry, DIL (Fig. 3). The density of ferrites determined before the dilatometric measurement was successively amounted to 2770, 2730 and 2690 kg m^{-3} for *S*1, *S*2 and *S*3, respectively. The smallest shrinkage, and in consequence density, was observed for the material obtained from the oxalate precipitate (*S*1). The shrinkage was only 5.6% and the densification process started at much higher temperature (1050 °C) than for the other samples. This high temperature, in which the material undergoes shrinkage, is not favorable due to lower final density. For comparison, the ferrites obtained from the carbonate (*S*2) and hydroxide precipitate (*S*3), whose densification processes started at 830 and 700 °C, had a significantly higher shrinkage (21.8 and 21.7%). The density of samples (after final sintered toroid) was determined based on the Archimedes' principle. The density of *S*1 sample amounted to 4189 kg m^{-3} and differed significantly from the density of Mn–Zn ferrite (4900 kg m^{-3}) commercially produced [36]. The shrinkage for *S*2 and *S*3 is similar to ferrite produced commercially by ceramic method (shrinkage amounted at about 20%), and these samples were characterized by higher final density: 4412 and 4355 kg m^{-3} for *S*2 and *S*3, respectively. A slightly lower density (4355 kg m^{-3}) of material prepared from carbonate precipitate (*S*2) may be due to higher densification temperature.

For better characterization of the microstructure and magnetic properties of the ferrites obtained from the spent battery leach solution, they were compared with reference

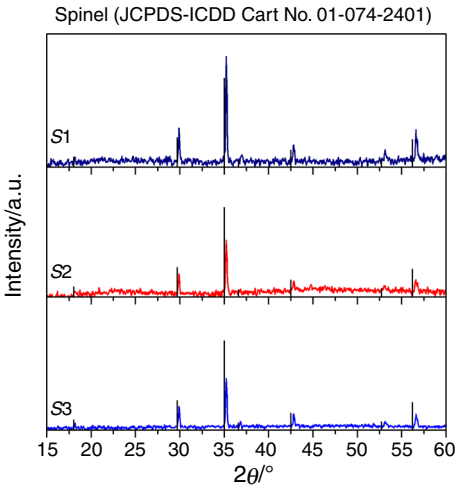

Fig. 2 The XRD diffraction patterns of Mn–Zn ferrites sintered at 1325 °C

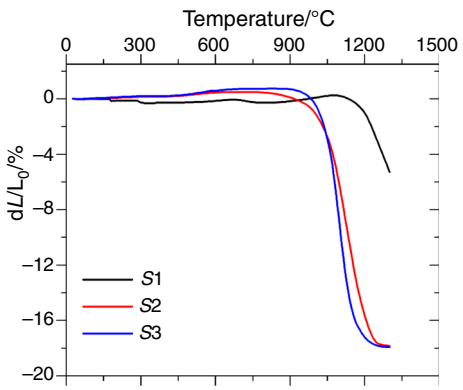

Fig. 3 The temperature dependence of linear shrinkage on compressed ferrite material

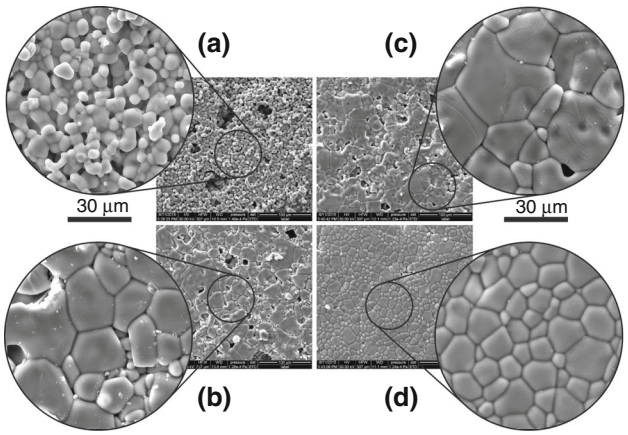

Fig. 4 SEM microphotographs of prepared Mn–Zn ferrite **a** *S*1, **b** *S*2, **c** *S*3, **d** HighPerm grade from Ferroxcube

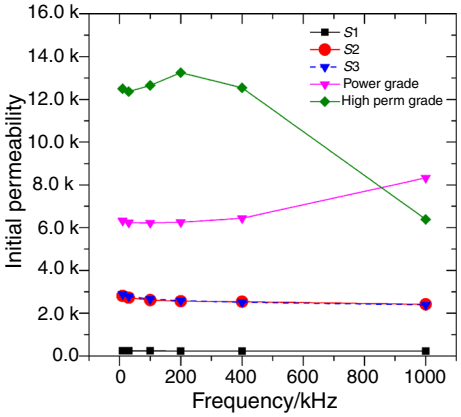

Fig. 5 Relative initial permeability as a function of frequency (0.1 mT, 25 °C)

samples received from Ferroxcube. As it is shown in Fig. 4, the morphology of ferrites prepared after pressing and sintering at high temperature is diverse. The ferrite obtained from oxalate precursor (*S*1) is characterized by fine and homogeneous microstructure. The grain is roughly spherical, with size less than 5 µm (Fig. 4a). It can be seen in the magnification inter grains are free spaces and pores. The pronounced porosity results from insufficient densification are reflected in low density. On the other hand, Mn–Zn ferrite prepared from carbonate (*S*2) and hydroxide (*S*3) precursors is characterized by non-uniform microstructure, which consists of grains different in size (Fig. 4b, c). An abnormal, exaggerated grain growth effect favors intergranular pore formation. The promoter of the duplex structures formation can be the presence of SiO_2 in larger quantities [37]. By contrast, the reference sample from Ferroxcube obtained by conventional ceramic method (Fig. 4d) possesses comparatively homogeneous microstructure. Pores or gaps are not visible, which means that material is compacted properly. However, grains are

Table 2 Magnetic properties of ferrites prepared by co-precipitation and conventional ceramic method (reference samples)

Measurement conditions	Temperature/°C	Sample			FXC reference sample	
		*S*1	*S*2	*S*3	Power grade[a]	HighPerm grade[a]
Initial permeability						
10 kHz; 0.1 mT	10	226	2649	2605	5694	11,352
30 kHz; 0.1 mT	25	237	2799	2887	6330	12,500
100 kHz; 0.1 mT	40	248	2963	3226	7255	13,452
200 kHz; 0.1 mT	55	259	3080	3626	8361	14,134
400 kHz; 0.1 mT	70	268	3151	4120	9623	14,734
1000 kHz; 0.1 mT	85	275	3150	4696	10,853	15,403
Loss factor						
100 kHz; 0.1 mT	25	–	–	–	–	0.9
200 kHz; 0.1 mT	25	–	–	–	–	8.4
400 kHz; 0.1 mT	25	–	23	23	1	29
1000 kHz; 0.1 mT	25	110	118	62	26	164
Power loss/mW cm^{-3}						
25 kHz; 200 mT	25	2390.7	Not able to measure	Not able to measure	31.8	14.1
	90	5143.6			5.9	26.8
	95	5559.6			4.3	28.8
	100	6350.7			4.1	30.8
	105	6727.9			4.7	33.8
	110	7394.2			5.3	38.6

[a]Commercially available ring core—Ferroxcube

relatively large in the range of 5–20 μm. Such differences between the microstructure of materials obtained from battery waste and those synthesized by the traditional ceramic method explain the deterioration of the magnetic properties of the former ferrites (see Table 2, Fig. 5).

Magnetic properties were investigated on EMMA device. An initial permeability (μ_i), loss factor ($tg\ \delta/\mu_i$) and power loss (P_v) were measured and are summarized in Table 2. The samples *S*2 and *S*3 display high values of initial permeability; however, these values are almost twice lower than reference sample "Power grade" (from Ferroxcube). The initial permeability for sample *S*1 was definitely lower, but independent of frequency and temperature. Figure 5 shows relationships between initial permeability and frequency at 25 °C, and in this case, sample *S*1 is characterized also by lowest permeability. Samples *S*2 and *S*3 exhibit comparable values of initial permeability, slightly changing with frequency. It is interesting to note that the obtained values of initial permeability correspond quite well to results described in the literature for ferrites synthesized by co-precipitation method [38]. Mangalaraja et al. [6] suggested that the low initial permeability value for materials prepared by chemical method can be associated with higher value of anisotropy constant and microstructure of prepared ferrite (grains size, grain and pore distribution). Low value of initial permeability for samples prepared from waste battery scrap can be a result of the presence of intergranular pores, which in the magnetic field holds the domain walls back to the rotation.

Power loss was measured at frequency of 25 kHz and magnetic field 200 mT. The *S*2 and *S*3 samples are characterized by high power loss and the measurements were unfeasible. Power loss for sample *S*1 was measured; however, it was still higher than that for reference samples. The studied materials were characterized by loss factor ($tg\ \delta/\mu_i$) at higher frequency comparable to samples from Ferroxcube. The loss factor value in Mn–Zn ferrites depends on composition (relation between Fe_2O_3, MnO and ZnO) and microstructure. Kogias et al. [39] explained that lower sintered density reduces the magnetic flux per unit volume, reduces μ_i and increases P_v. In order to prepare ferrite characterized by low losses at high frequencies, it is necessary to choose both composition and additives which will minimize constant anisotropy and will produce a material with uniform grain size, without defects, pores or impurities [40].

Conclusions

Mn–Zn ferrites obtained by co-precipitation from the acid solution after leaching of the waste batteries differ in microstructure and magnetic properties according to the precipitant used. DTA–TGA study indicates thermal decomposition of precipitants at low temperature (200–400 °C) with mass change. For all samples, slightly exothermic effect connected with an α-hematite phase transformation to spinel at DTA curve is visible. The phase transformation was also confirmed in XRD studies. The α-hematite is present in powders after pre-sintering step, whereas after final pressing and high-temperature sintering at 1325 °C only ferrite phase appears at XRD spectra. Ferrite powders prepared after co-precipitation have been subjected to typical processing (grinding-pressing-sintering) as commercial produced materials. Ferrites prepared from carbonate and hydroxide precipitant show shrinkage similar to ferrite produced on an industrial scale (about 20%). However, an exaggerated grain growth effect and intergranular pores in pressed ferrites (*S*2 and *S*3) caused lower initial permeability, which changes with frequency in the same way for these samples. Ferrite toroid prepared from oxalate precursor possesses lower shrinkage (only 5.6%), lower density but uniform and fine microstructure. The initial permeability for this sample was definitely lower, but independent of frequency and temperature. The results of magnetic testing compared to commercial ferrites are not fully satisfactory. However, optimization of the pressing and sintering processes of such fine powders could in future contribute to better compaction. The selection of additives to reduce excessive grain growth in samples obtained from the hydroxide and carbonate precursors would contribute to more uniform microstructure. The reduction in these samples of power losses with a similar permeability value would allow to use them in power switching application. A slight shrinkage of the sample obtained from the oxalate precursor for application reasons appears to be interesting as it allows the possibility of designing a material with a large tolerance of shape.

Acknowledgements The authors would like to thank Magdalena Pawlak and Dietmar Holtz from Ferroxcube for the magnetic measurements and the assistance provided.

References

1. Verma RK, Singh RK, Narayan A, Verma L, Singh AK, Kumar A, Pathak PK, Aman AK. Low-temperature synthesis of hexagonal barium ferrite ($BaFe_{12}O_{19}$) nanoparticles by annealing at 450 °C followed by quenching. J Therm Anal Calorim. 2017;129:691–9.
2. Azadmanjiri J. Preparation of Mn–Zn ferrite nanoparticles from chemical sol–gel combustion method and the magnetic properties after sintering. J Non Cryst Solids. 2007;353:4170–3.
3. Waqas H, Qureshi AH. Low temperature sintering study of nanosized Mn–Zn ferrites synthesized by sol–gel auto combustion process. J Therm Anal Calorim. 2010;100:529–35.
4. Szczygiel I, Winiarska K. Low-temperature synthesis and characterization of the Mn–Zn ferrite. J Therm Anal Calorim. 2011;104:577–83.
5. Coutinho DM, Verenkar VMS. Preparation, spectroscopic and thermal analysis of hexa-hydrazine nickel cobalt ferrous succinate precursor and study of solid-state properties of its nanosized thermal product, $Ni_{0.5}Co_{0.5}Fe_2O_4$. J Therm Anal Calorim. 2017;128:807–17.
6. Mangalaraja RV, Ananthakmar S, Manohar P, Gnanam FD, Awano M. Characterization of $Mn_{0.8}Zn_{0.2}Fe_2O_4$ synthesized by flash combustion technique. Mater Sci Eng A. 2004;367:301–5.
7. Arulmurugan R, Vaidyanathan G, Sendhilnathan S, Jeyadevan B. Mn–Zn ferrite nanoparticles for ferrofluid preparation: study on thermal-magnetic properties. J Magn Magn Mater. 2006;298:83–94.
8. Cao X, Liu GA, Wang YM, Li JH, Hong RY. Preparation of octahedral shaped $Mn_{0.8}Zn_{0.2}Fe_2O_4$ ferrites via co-precipitation. J Alloy Compd. 2010;497:L9–12.
9. Rath C, Sahu KK, Anand S, Date SK, Mishra NC, Das RP. Preparation and characterization of nanosize Mn–Zn ferrite. J Magn Magn Mater. 1999;202:77–84.
10. Nalbandian L, Delimitis A, Zaspalis VT, Deliyanni EA, Bakoyannakis DN, Peleka EN. Hydrothermally prepared nanocrystalline Mn–Zn ferrites: synthesis and characterization. Microporous Mesoporous Mater. 2008;114:465–73.
11. Păcurariu MSC, Muntean E-C. Thermal stability of the solvothermal-synthesized $MnFe_2O_4$ nanopowder. J Therm Anal Calorim. 2017;127:155–62.
12. Mathew DS, Juang RS. An overview of the structure and magnetism of spinel ferrite nanoparticles and their synthesis in microemulsions. Chem Eng J. 2007;129:51–65.
13. Dasgupta S, Kim KB, Ellrich J, Eckert J, Manna I. Mechanochemical synthesis and characterization of microstructure and magnetic properties of nanocrystalline $Mn_{1-x}ZnFe_2O_4$. J Alloy Compd. 2006;424:13–20.
14. Tatarchuk T, Bououdina M, Vijaya J, Kennedy JL. Spinel ferrite nanoparticles: synthesis, crystal structure, properties, and perspective applications. Springer Proc Phys. 2017;195:305–25.
15. Shah SA, Majeed A, Rashid K, Awan SU. PEG-coated folic acid-modified superparamagnetic $MnFe2O_4$ nanoparticles for hyperthermia therapy and drug delivery. Mater Chem Phys. 2013;138:703–8.
16. Ito A, Shinkai M, Honda H, Kobayashi T. Medical application of functionalized magnetic nanoparticles. J Biosci Bioeng. 2005;100:1–11.
17. Le Guével X, Prinz EM, Müller R, Hempelmann R, Schneider M. Synthesis and characterization of superparamagnetic nanoparticles coated with fluorescent gold nanoclusters. J Nanopart Res. 2012;14:727–37.
18. Sharifi I, Shokrollahi H, Amiri S. Ferrite-based magnetic nanofluids used in hyperthermia applications. J Magn Magn Mater. 2012;324:902–15.
19. Winiarska K, Szczygieł I, Klimkiewicz R. Manganese-zinc ferrite synthesis by the sol–gel autocombustion method. Effect of the precursor on the ferrite's catalytic properties. Ind Eng Chem Res. 2013;52:353–61.
20. Winiarska K, Klimkiewicz R, Winiarski J, Szczygieł I. $Mn_{0.6}Zn_{0.4}Fe_2O_4$ ferrites prepared by the modified combustion method as the catalyst for butan-1-ol dehydrogenation. React Kinet Mech Cat. 2017;120:261–78.
21. Nan JM, Han DM, Cui M, Yang MJ, Pan LM. Recycling spent zinc manganese dioxide batteries through synthesizing Zn–Mn ferrite magnetic materials. J Hazard Mater B. 2006;133:257–61.
22. Peng CH, Bai BS, Chen YF. Study on the preparation of Mn–Zn soft magnetic ferrite powders from waste Zn–Mn dry batteries. Waste Manag. 2008;28:326–32.
23. Liu CW, Lin CH, Fu YP. Characterization of Mn–Zn ferrite prepared by a hydrothermal process from used dry batteries and waste steel pickling liquor. J Am Ceram Soc. 2007;90:3349–52.
24. Xi GX, Yang L, Lu MX. Study on preparation of nanocrystalline ferrites using spent alkaline Zn–Mn batteries. Mater Lett. 2006;60:3582–5.
25. Gabal MA, RAl-luhaibi RS, Al Angari YM. Recycling spent zinc–carbon batteries through synthesizing nano-crystalline Mn–Zn ferrites. Powder Technol. 2014;258:32–7.
26. Kim TH, Kang JG, Sohn JS, Rhee KI, Lee SW, Shin SM. Preparation of Mn–Zn ferrite from spent zinc–carbon batteries by alkali leaching, acid leaching and co-precipitation. Mat Mater Int. 2008;14:655–8.
27. Kim TH, Senanayake G, Kang JG, Sohn JS, Rhee KI, Lee SW, Shin SM. Reductive acid leaching of spent zinc–carbon batteries and oxidative precipitation of Mn–Zn ferrite nanoparticles. Hydrometallurgy. 2009;96:154–8.
28. Xiai L, Zhou T, Meng J. Hydrothermal synthesis of Mn–Zn ferrites from spent alkaline Zn–Mn batteries. Particulogy. 2009;7:491–5.
29. Hu P, Pan DD, Zhang SG, Tian JJ, Volinsky AA. Mn–Zn soft magnetic ferrite nanoparticles synthesized from spent alkaline Zn–Mn batteries. J Alloy Compd. 2011;509:3991–4.
30. Directive 2006/66/CE of 6 September 2006 on Batteries and accumulators and waste batteries and accumulators. http://eur-lex.europa.eu/LexUriServ/LexUriServ.do?uri=OJ:L:2006:266:0001:0014:en:PDF.
31. Sobianowska-Turek A, Szczepaniak W, Zabłocka Malicka M. Electrochemical evaluation of manganese reducers—recovery of Mn from Zn–Mn and Zn–C battery waste. J Power Sources. 2014;270:668–74.
32. Sobianowska-Turek A, Ulewicz M, Grudniewska KL. Ion flotation and solvent sublation of zinc(II) and manganese(II) in the presence of proton-ionizable lariat ethers. Physicochem Probl Miner Process. 2016;52:1048–60.
33. Schaller GE. Ferrite processing & effects on material performance. http://www.cmi-ferrite.com/news/Articles/ferpro.pdf. Accessed 01 April 2018.
34. Morineau R, Paulus M. Chart of pO_2 versus temperature and oxidation degree for Mn–Zn ferrites in the composition range: 50 $< Fe_2O_3 <$ 54; 20 $<$ MnO $<$ 35; 11 $<$ ZnO $<$ 30 (mole percent). IEEE Trans Magn. 1975;11:1312–4.
35. Senanayake G, Shin S-M, Senaputra A, Winn A, Pugaev D, Avraamides J, Sohn J-S, Kim D-J. Comparative leaching of spent zinc–manganese–carbon batteries using sulfur dioxide in ammoniacal and sulfuric acid solutions. Hydrometallurgy. 2010;105:36–41.
36. Soft ferrites and accessories. Data Handbook. Ferroxcube. 2013. https://www.ferroxcube.com/en-global/download/index/product_catalog. Accessed 01 April 2018.
37. Goldman A. Modern ferrite technology. 2nd ed. Pittsburgh: Spinger; 2006.
38. Mathur P, Thakur A, Singh M. Low temperature processing of Mn–Zn nanoferrites. J Mater Sci. 2007;42:8189–92.
39. Koias G, Holtz D, Zaspalis V. New Mn–Zn ferrites with high saturation flux density. J Jpn Powder Powder Metal. 2014;61:201–3.
40. Liu YP, He SJ. Development of low loss Mn–Zn ferrite working at frequency higher than 3 MHz. J Magn Magn Mater. 2008;320:3318–22.